INCORPORATION OF LITHIUM ION ON Zn:CdS QUANTUM DOTS: STRUCTURAL AND OPTICAL INVESTIGATIONS

P. SAKTHIVEL[1], I. DEVADOSS[2], S.V. VIJAYASUNDARAM[3]

[1] Department of Physics, Faculty of Engineering, Karpagam Academy of Higher Education, Coimbatore 641021,Tamilnadu, India
E-mails: sakthi1807@gmail.com; sakthivel.p@kahedu.edu.in
[2] PG and Research Department of Physics, Bishop Heber College, Tiruchirappalli – 620017, Tamilnadu, India
[3] Department of Physics, E.G.S. Pillay Arts and Science College, Nagapattinam – 611002, Tamilnadu, India

Received February 13, 2020

Abstract. Zn and Li doped CdS quantum dots were fabricated *via* the co-precipitation method. X-ray diffraction, UV-Visible, *Fourier transformed infrared* (FTIR), photoluminescence studies were carried out. The obtained results, reveal cubic crystal structure, blue shifted optical band gap and red photoluminescence emission. The studied material will be suitable for optoelectronic applications.

Key words: Li-doped CdZnS, band gap tailoring, Photoluminescence

1. INTRODUCTION

Semiconducting nanomaterials are of the popular interest in recent days due to their size-dependent optical, electronic, magnetic, chemical, electrical, and mechanical properties, which usually don't occur in their bulk counterparts [1, 2]. Among semiconductors, A_{II}–B_{VI} semiconducting compounds receive more attention from the researchers around the globe because of the wide opportunities in tuning the properties for diverse applications [3]. *Quantum dots* (QDs) are generally defined as zero-dimensional semiconducting nanoparticles and their sizes are ranged from 1 nm to 10 nm. QDs are highly fascinating for labeling, imaging and optoelectronic applications. In the recent years, CdS is identified as popular QDs due to its notable properties. For instance, the band gap of CdS QDs is 2.4 eV, which is likely corresponding to the possibility of light absorption in the visible region [4]. Generally, the doping on CdS increases the sensing response and selectivity compared to the pristine CdS [5]. CdS is found to be useful material in optical, photoluminescent, optoelectronic including photovoltaic applications [6, 7]. Transition metals doping on Cds leads to drastic changes in the structural, optical, electrical, magnetic, and dielectric properties. Zn offers the best option for a dopant because of its ionic size, affordability to mingle with host lattice and for a wide range of band gap tailoring [8]. Zn provides a gateway to the engineering of bipolar homojunction, *p*-type

transparent conductive materials and spintronics applications [9]. The doping of Zn in CdS resulted in a reduction in grain size and lattice parameter, but increase in optical transmittance [10]. The optical band gap was widened and electrical conductivity was improved due to the incorporation of Zn ions in CdS host [11]. The doping concentration of Zn is fixed as 10% in the present investigation since this composition ratio exhibited a better crystallinity and possessed a wide energy gap in the previous work [12]. Lithium is a monovalent element exhibiting a better electrical property [13]. Lithium-ion was used to modify the structural, surface morphological, optical, electrical, and ferroelectric properties of the target element [14, 15]. Lithium doped ZnS showed an enhancement in photoluminescence behavior [16]. To further tune the properties of Zn:CdS QDs, Lithium is chosen as a co-dopant. The $Cd_{0.9-x}Zn_{0.1}Li_xS$ (x = 0, 0.02, 0.04, 0.06) QDs were prepared by using co-precipitation method. This method is identified as an easy, cost-effective and higher yield method. The structural, morphological, elemental, compositional, optical, photoluminescence studies of $Cd_{0.9-x}Zn_{0.1}Li_xS$ (x = 0, 0.02, 0.04, 0.06) QDs were carried out and the results were discussed.

2. EXPERIMENTAL DETAILS

$Cd_{0.9-x}Zn_{0.1}Li_xS$ (x = 0 to 0.06) QDs were synthesized by using chemical co-precipitation method. The chemicals such as cadmium acetate dihydrate (Cd $(CH_3COOH)_2 \cdot 2H_2O$), zinc acetate dihydrate ($Zn(CH_3COOH)_2 \cdot 2H_2O$), lithium acetate dihydrate (Li $(CH_3COOH)_2 \cdot 2H_2O$) and sodium sulfide (Na_2S) were used as source materials of Cd^{2+}, Zn^{2+}, Li^{2+}, and S^{2-} ions, respectively. The chemicals are of high purity AR grade. They were purchased from Merck chemical Co. and used as purchased. In the preparation of $Cd_{0.9-x}Zn_{0.1}Li_xS$ QDs, the amount of precursors varies with the required concentration. For instance, while preparing $Cd_{0.84}Zn_{0.1}Li_{0.06}S$ QDs, 0.84 M cadmium acetate dihydrate, 0.1 M zinc acetate dihydrate and 0.06 M Lithium acetate dihydrate were slowly dissolved one by one in 50 ml double distilled water kept in the beaker A. The beaker B is used to prepare 1 M sodium sulfide solution using 50 ml water. Both the solutions were constantly stirred for 30 minutes to achieve clear and homogeneous solutions. Then, the sodium sulfide solution in the beaker B was slowly added dropwise to the solution in beaker A under constant stirring at room temperature. Aqueous ammonia was used to adjust the pH value to 9.5. Further, the final solution is continuously stirred for 2 h at room temperature to ensure the homogeneous reaction throughout the volume. Finally, the precipitate was filtered and then washed several times using double distilled water and ethanol to eliminate the impurities and acetate ions from the precipitates. The collected precipitates were dried using an oven at 80°C for 12 h. The end products were grounded using an agate mortar. In the similar fashion, the samples with different compositions such as

$Cd_{0.9}Zn_{0.1}S$ (CdZnS) $Cd_{0.9-x}Zn_{0.1}Li_xS$ (CdZnLiS) (x = 0.02, 0.04, 0.06) QDs were prepared. The crystal structures of the synthesized CdZnS and CdZnLiS QDs were characterized using a Rigaku C/max-2500 powder X-ray diffractometer with Cu Kα radiation (λ = 1.5406 Å) by applying 40 kV operating voltage and maintaining 60 mA current. XRD patterns are recorded in the range of 20–80° with a step of 0.02°. The transmission electron microscopy was served to record the pictures by using Philips – CM200 TEM with operating voltage from 20 to 200 kV. The morphology, elemental composition, and distribution of the particles on the surface of the synthesized nanoparticles are studied by using the *scanning electron microscope* (SEM) technique with the microscope (SEM, JEOLJSM 6390). The topological information and composition of Zn, Cd, S were determined by energy dispersive X-ray spectrometer. Ultraviolet-visible (UV-Vis) absorption and transmittance spectra were recorded by using a UV-Visible spectrophotometer (Model: lambda 35, Perkin Elmer) in the wavelength range from 300 nm to 600 nm for studying the optical properties of the synthesized samples. The presence of chemical bonding in the synthesized nanoparticles is studied by FTIR spectrometer (Model: Perkin Elmer, Make: Spectrum RXI) in the range of 400–4000 cm^{-1}. The *photoluminescence* (PL) spectra of both CdZnS and CdZnLiS nanoparticles were obtained with the wavelength ranging from 350 to 600 nm by using a fluorescence spectrophotometer (Model: Hitachi F-2500).

3. RESULTS AND DISCUSSION

3.1. STRUCTURAL STUDIES

The structural modification due to the effect of Li concentration was systematically investigated in Zn and Li co-doped CdS samples with the help of *X-ray diffraction* (XRD) studies. Figure 1a shows the XRD patterns of the processed co-doped samples. The figure explicitly reveals one strong diffraction peak (2θ = 27.2°) and two weak diffraction peaks (2θ = 44.3 and 52.4°), which could be the reflections from (111), (220) and (311) planes of CdS cubic phase, respectively [17]. CdS can naturally crystallize in two different crystal structures: hexagonal (wurtzite) and cubic (zinc blende). However, the chemical reaction at room temperature yields a heterogeneous process with a simple cubic structure [18, 19]. The initial substitution of Li in Zn:CdS host lattice made a slight shift in 2θ value towards the lower angle side and a further increase of Li composition gradually shifted the primary peak position to a higher angle side. This shift of primary peak position ensured the inclusion of Li-ion in the target lattice. The reflections closely match with the JCPDS card no. 65–2887, which is in good agreement with the past reports on CdS system [20]. It is noted that no other phases

corresponding to metal, oxides or sulfide (such as Zn, Cd, ZnS, ZnO, CdO, ZnO, etc.) were detected. The absence of other phases ensures the purity of the desired co-doped phase in each sample. The development of the desired phase could be attributed to the following reasons: The ionic radius of the dopant Zn^{2+} (0.60 Å) is smaller than that of Cd^{2+} (0.97 Å). Hence, Cd^{2+} can be very well replaced by Zn^{2+} ions [21]. Li, being the other dopant, would also be substituted very well in the lattice of CdS due to its lower ionic radius (0.68 Å) than Cd ion [22]. Besides, it is expected that Li ions not only substitute Cd ions but occupy some interstitial lattice sites in Cd-Zn-S.

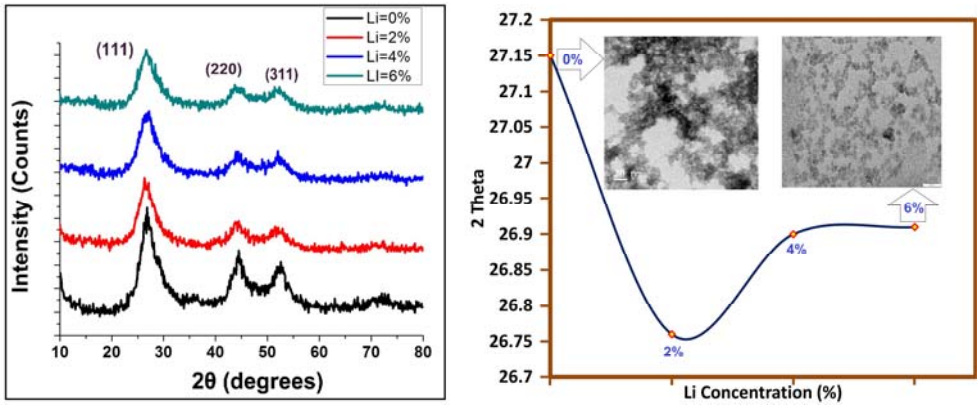

Fig. 1 – (Color online) a) XRD patterns of $Cd_{0.9-x}Zn_{0.1}Li_xS$ samples,
b) Variation of particle size *vs* Li concentration.

The substituted Li-ions at Cd lattice sites resulted in a decrease of the grain size, lattice constant and the (111) crystalline plane distance. In comparison with the Zn-doped CdS sample (CdZnS), both Zn and Li doped (CdZnLiS) samples have relatively lower diffracted intensity along (111) plane. This observation confirms that Li ions are doped into Cd-Zn-S lattice successfully [23]. Further, the intensities of (111) planes of the XRD patterns decreased with Li concentration, and exactly opposite to the trend in the FWHM of (111) diffraction peaks that reach a minimum of about 0.24° at 6%. From the earlier reports, it is noted that when Zn replaces Cd, there arises a phase transition from hexagonal to cubic with an increase of Zn content. However, the inclusion of Li ions leads to only a small alteration in the structure of the compound, not significantly. This is evident from the observed identical diffraction of all co-doped samples. The appropriate background-corrected X-ray data is used to calculate the average crystallite size (D) of the QDs using Debye-Scherrer's formula [24]. Average crystallite size:

$$(D) = 0.9\lambda / \beta \cos \theta \quad (1)$$

The developed micro-strain (ε) in the nanoparticles are calculated by using the formula, Micro-strain

$$(\varepsilon) = \beta \cos\theta / 4 \tag{2}$$

Table 1 shows the information of the peak position (2θ), *full width at half maximum* (FWHM, β), d value, lattice parameter, the average crystallite size (D) and micro-strain (ε) of $Cd_{0.9-x}Zn_{0.1}Li_xS$ nanoparticles for different Li concentrations from 0% to 6%. The average crystallite size is reduced from 2.10 nm to 1.99 nm due to the compositional variation of Li doping as mentioned above. It is concluded from Table 1 that there is a changing in crystallite size with Li concentration 0% to 6%. Further, the micro-strain of the Li doped samples gradually increases after a small decrease for the 2% Li doped sample. The increase of strain causes the decrease of lattice parameters and average crystallite size. This increase of micro-strain is responsible for the broadening of diffraction peaks [25]. Figure 1b shows the variation of particle size as a function of Li concentration. The inset TEM picture reveals the structure of particles before and after incorporation of Li in Zn:CdS QDs.

Table 1

The peak position (2θ), full width at half maximum (FWHM, β) value, d-value, lattice parameter average crystalline size (D) and micro strain (ε) along (111) plane of $Cd_{0.9-x}Zn_{0.1}Li_xS$ (x = 0, 0.02, 0.04, 0.06) quantum dots

Samples	**Peak position (2θ)(°)**	**FWHM (β)**	**$d_{(111)}$ (Å)**	**Lattice parameter (Å)**	**Crystallite size (D) (nm)**	**Micro strain (ε) × 10^{-3}**
$Cd_{0.90}Zn_{0.10}S$	27.15	3.89	3.28	5.680	2.10	16.50
$Cd_{0.89}Zn_{0.10}Li_{0.02}S$	26.76	3.69	3.33	5.767	2.21	15.65
$Cd_{0.87}Zn_{0.10}Li_{0.04}S$	26.90	4.13	3.31	5.732	1.98	17.50
$Cd_{0.85}Zn_{0.10}Li_{0.06}S$	26.91	4.10	3.30	5.715	1.99	17.39

3.2. MICRO-STRUCTURAL STUDIES

Figure 2 depicts the SEM images of all the synthesized Li doped Cd-Zn-S samples. All the samples look uniform morphologies with good crystalline nature. The decreasing grain sizes of the samples with increasing Li concentration is evident from the microstructural images. The surface passivation was increased because of small-sized particles gathering on the surface. Lithium-ion incorporation raised the accumulation of small grains with CdS particles.

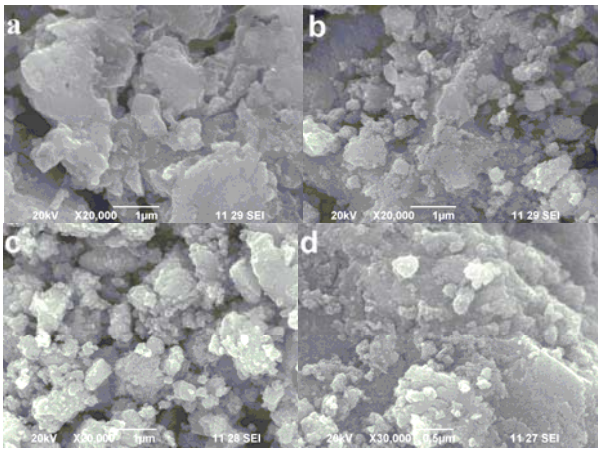

Fig. 2 – (Color online) SEM images of $Cd_{0.9-x}Zn_{0.1}Li_xS$ samples.

3.3. EDAX ANALYSIS

Figure 3 illustrates the surface morphology of Zn doped CdS and Li+Zn co-doped CdS QDs. The atomic weight quantities of Zn, Cd, S are present as per the stoichiometry ratio. Li was undetected even for higher composition (6%) by using this instrument as Li is a lighter element. NMR spectroscopic technique can be used to detect the existence of Li in the co-doped CdS QDs.

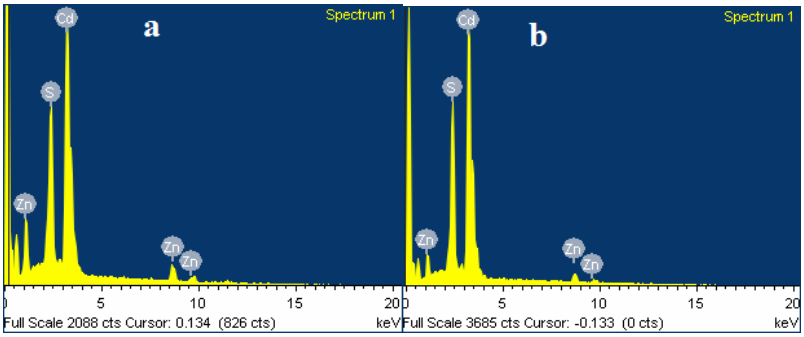

Fig. 3 – (Color online) a) EDAX image of $Cd_{0.9-x}Zn_{0.1}S$ QDs, b) $Cd_{0.9-x}Zn_{0.1}Li_{0.02}S$ QDs

3.4. UV-VIS SPECTRAL STUDIES

The optical absorption and transmittance spectra of synthesized CdZnS and CdZnLiS compounds were recorded by using a UV-Vis spectrometer in the ultraviolet-visible range 300–600 nm.

The UV-Vis absorption spectra in the Fig. 4a reveals that the ultraviolet cut-off (~335 nm) absorption of CdZnLiS compounds shifts to higher energy compared to

CdZnS. The observed absorption found at the shorter wavelength (blue shift) regions represents an increase in the band gap caused by the change in crystallite size associated with the inclusion of Li ions. Thus, the blue shift of absorption edge, compared to its bulk counterparts, evidently describes the quantum confinement effect of the QDs [26]. The UV-Vis transmittance spectra were illustrated in the Fig. 4b. All the transmittance peaks of CdZnLiS were suppressed than CdZnS QDs.

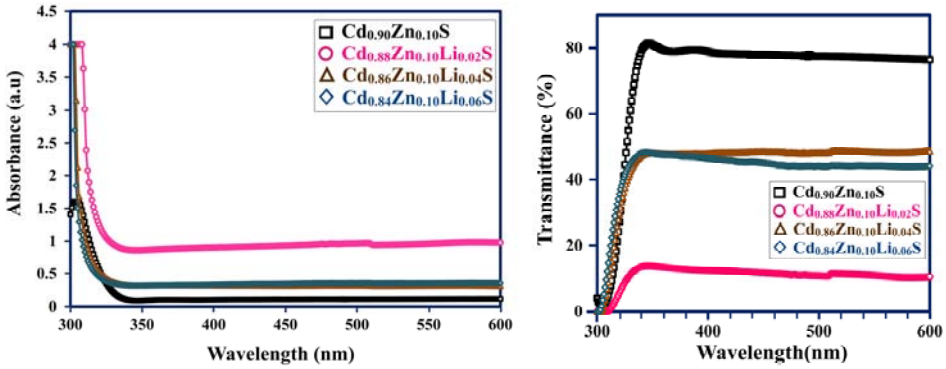

Fig. 4 – (Color online) UV-Vis spectra of $Cd_{0.9-x}Zn_{0.1}Li_xS$ samples: a) Absorbance, b) Transmittance.

The optical band gap energy (E_g) of the synthesized QDs can be estimated using the Tauc plot of $(h\nu\alpha)^2$ *vs.* ($h\nu$) and the extrapolation of the linear portions of the curves to the energy axis according to [27]:

$$\alpha h\nu = A(h\nu - E_g)^{1/2} \tag{3}$$

where α is the absorption coefficient, $h\nu$ is the photon energy, E_g is the direct band gap energy, and A is a constant. From the above relation, observed optical band gap energy of these compositions varies from 3.88 – 4.04 eV as shown in the Fig. 4c.

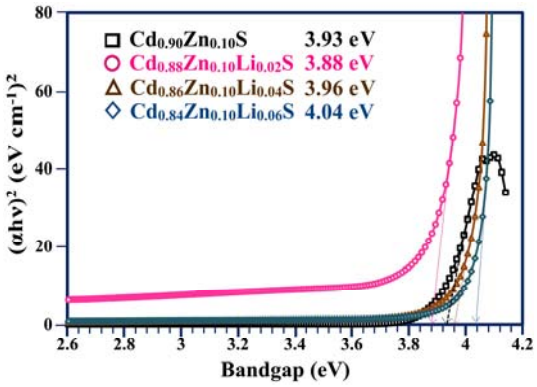

Fig. 4c – (Color online) Tauc plot of $(h\nu\alpha)^2$ *vs.* ($h\nu$).

3.5. PHOTOLUMINESCENCE ANALYSIS

Figure 5 shows the room temperature *photoluminescence* (PL) spectra of the CdZnS and CdZnLiS QDs observed with the excitation wavelength of 330 nm. The PL spectra clearly show that the peak corresponding to the red region falls at 640 nm for CdZnS QDs. However, the PL peaks of CdZnLiS samples are shifted to nearly 675 nm. This shift in CdZnLiS samples could be attributed to a strong interaction between the Zn3d- and Li2s- orbitals due to the considerably high ionization energy of Lithium [28]. The increase of Li concentrations in association with the cationic d-orbitals of Zn promotes high chemical stability in the CdZnLiS samples, and thus there are an accountable increase in the band gap energy (Fig. 4c) and decrease in the luminescence peak intensity of those samples. The similar fashioned narrow peaks with FWHM less than ~20 nm have been reported for various undoped semiconducting nanoparticles, which exhibit better luminescence intensity [29, 30].

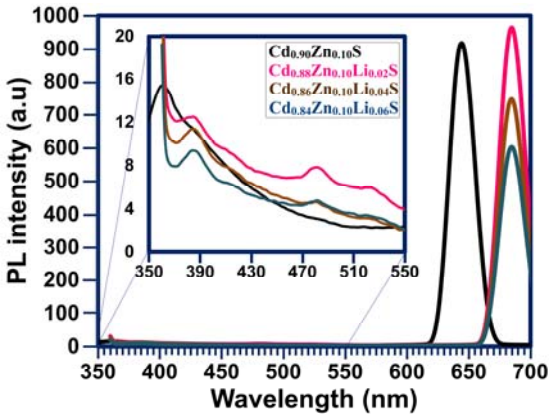

Fig. 5 – (Color online) Photoluminescence spectra of $Cd_{0.9-x}Zn_{0.1}Li_xS$ samples.

3.6. FTIR SPECTRAL STUDIES

Figure 6 shows the FT-IR spectra of the CdZnS and CdZnLiS QDs recorded in the frequency range 400–4000 cm^{-1}. The broad peak centered at 3440 cm^{-1} is attributed to the O–H stretching vibration due to the presence of moisture [31]. Higher transmittance is achieved for Li = 6% from about 1800 cm^{-1} to 3000 cm^{-1}. The peaks received near 1420 cm^{-1} is ascertained to C=O stretching vibrations. The bands observed around 1018 cm^{-1} are owing to C=O stretching vibrations due to the absorption of acetates by the surface of the synthesized QDs [32]. A strong band position observed at 1580 cm^{-1} is assigned to the stretching vibrations of the sulfate group. The absorption at 605 cm^{-1} shows the presence of Cd–S stretching vibration [33].

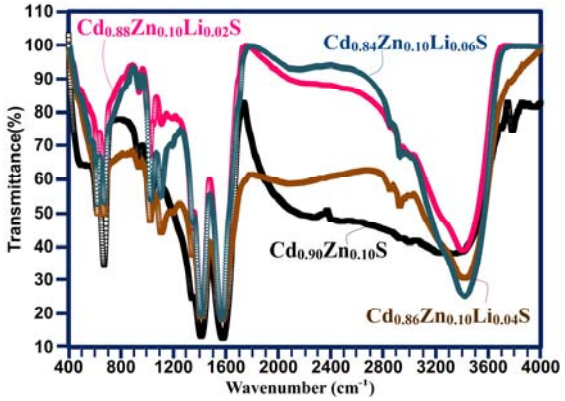

Fig. 6 – (Color online) FT-IR spectra of $Cd_{0.9-x}Zn_{0.1}Li_xS$ samples.

There is no significant change in the peak position of CdZnLiS due to Li doping. It shows that the Li crystallites are independent, formed without disturbing the continuous 3-D matrix of the CdZnS. However, it contributes to the synthesis of the samples in the nano-scale.

4. CONCLUSIONS

$Cd_{0.9-x}Zn_{0.1}Li_xS$ (x = 0, 0.02, 0.04, 0.06) QDs were synthesized successfully through chemical co-precipitation method. XRD results affirmed the existence of cubic structure of the samples without the creation of any secondary phases. The sizes of the synthesized QDs decreased due to the inclusion of Li in Zn:CdS. TEM Photographs revealed that the samples possess the clusters of spherically shaped tiny particles. FTIR and EDAX analyses confirmed the elements present in the prepared samples and its purity. UV–Vis absorption intensity was increased as a function of Li incorporation. Band gap energy was blue shifted (4.04 eV from 3.94 eV) due to quantum confinement effect and the wide energy gap was observed for the doping concentration of Li = 6%. The photoluminescence emission peaks received in UV and Red region were shifted to higher wavelength because of Li incorporation. This shifting of peaks was attributed to band transition between Li and Zn. Since these materials have high optical absorption, wide band gap, better photoluminescence, they could serve for optoelectronic applications including solar cells.

REFERENCES

1. M. Gu, Q. Zhang and S. Lamon, Nat. Rev. Mater **1**, 16070 (2016).
2. M. Bangal, S. Ashtaputre, S. Marathe, A. Ethiraj, N. Hebalkar, S. W. Gosavi, J. Urban and S. K. Kulkarni, Hyperfine Interact. **160**, 81 (2005).

3. J. Jie, W. Zhang, I. Bello, C-S. Lee and S-T. Lee, Nano today **5**, 313 (2010).
4. C. J. Murphy, Anal. Chem. **74**, 520A (2002).
5. N. Zhang, X. Ma, S. Ruan, Y. Yin, C. Li, H. Zhang, and Y. Chen, J. Nanosci. Nanotechnol. **19**, 7083 (2019).
6. S. Antohe, Sorina Iftimie, Veta Ghenescu, Raluca Constantineanu, M.M. Gugiu, M. Ion, I. Stan, A. Radu, L. Ion, Romanian Reports in Physics, **64**, 1153 (2012).
7. O. Toma, L. Ion, S. Iftimie, V. A. Antohe, A. Radu, A. M. Raduta, D. Manica, S. Antohe, App. Surf. Sci. **478**, 831(2019).
8. X. Fang, T. Zhai, U.K. Gautam, L. Li, L. Wu, Y. Bando and D. Golberg, Prog. Mater. Sci. **56**, 175 (2011).
9. P. D'Amico, A. Calzolari, A. Ruini and A. Catellani, Sci. Rep. **7**, 16805 (2017).
10. A. A. Ibiyeni, A. O. Awodugba, O. Akinrinola and A. A. Faremi, J. Semicond. **38**, 093002 (2017).
11. L. Ma, X. Ai and X. Wu, J. Alloys Compd. **691**, 399 (2017).
12. I. Devadoss, S. Muthukumaran and M. Ashokkumar, J. Mater. Sci. Mater Electron **25**, 3308 (2014).
13. W.L. Yang, Y.M. Lu, W.S. Hwang and W.C. Chen, J. Eur. Ceram. Soci. **30**, 503 (2010).
14. S. Majumdar and P. Banerji, Superlattices Microstruct. **45**, 583 (2009).
15. S. Aksoy, Y. Caglar, S.Ilican and M. Caglar, J. Alloys Compd. **512**, 171 (2012).
16. S. Nakumara, J. Yamaguchi, S. Takagimoto, Y. Yamada and T. Taguchi, J. Cryst. Growth **237**, 1570 (2002).
17. S. Horoz and O. Sahin, J. Mater. Sci. Mater. Electron. **28**, 17784 (2017).
18. S. Arora and S. S. Manoharan, Opt. Mater. **31**, 176 (2008).
19. N. A. Al-Tememee, N. M. Saeed, S. M. A. Al-Dujayli and T. C. Baha, Adv. Mater. Phys. Chem. **2**, 69 (2012).
20. U. Sandoval, M. E. H. Tones, J. M. G. Jimenez and N. K. Silva Gonzalez, Mater. Res. Soc. Symp. Proc. 1509 (2013). DOI:10.1557/opI. 2 013. 554.
21. I. Carreón-Moncada, L. A. González, M. I. Pech-Canul and R. Ramírez-Bon, Thin Solid Films **548**, 270 (2013).
22. P. Samiyammal, K. Parasuraman and A.R. Balu, Superlattices and Microstruct. **129**, 28 (2019).
23. N. S. Gajbhiye, R. S. Ningthoujam, A. Ahmed, D. K. Panda, S. S. Umare and S. J. Sharma, Pramana **170**, 313 (2008).
24. R. Kumar, P. Sakthivel and P. Mani, App. Phys. A **125**, 543 (2019).
25. I. Devadoss and S. Muthukumaran, Physica E **72**, 111 (2015).
26. R. Seoudi, A. Shabaka, W. H. Eisa, B.Anies and N. M. Farage, Physica B **405**, 919 (2010).
27. P. Sakthivel, T. Jayasri, J. Madhumitha, S. Mahalakshmi and N. Subhashini, Optik **154**, 74 (2018).
28. S. H. Wei and A. Zunger, Appl. Phys. Lett. **72**, 2011 (1998).
29. H. Weller, Curr. Top. Coll. Int. Sci. **3,** 194 (1998).
30. S. Salimian and S. Farjami Shayesteh, Acta Physica Polonica A **118**, 632 (2010).
31. P. Sakthivel and S. Muthukumaran, J. Inorg. Organomet Polym. **26**, 563 (2016).
32. I. Devadoss., P. Sakthivel, S. Muthukumaran and N. Sudhakar., Ceram. Int. **453**, 3833 (2019).
33. N. Kumar, L. P. Purohit and C. Goswami, Chalcogenide Letters **12**, 333 (2005).